

Hutchinson-Gilford Progeria Is a Skeletal Dysplasia

Catherine M Gordon,¹ Leslie B Gordon,^{2,3} Brian D Snyder,^{4,5} Ara Nazarian,⁵ Nicolle Quinn,⁶ Susanna Huh,⁷ Anita Giobbie-Hurder,⁸ Donna Neuberger,⁹ Robert Cleveland,¹⁰ Monica Kleinman,³ David T Miller,¹¹ and Mark W Kieran¹²

¹Divisions of Adolescent Medicine and Endocrinology, Children's Hospital Boston, Harvard Medical School, Boston, MA, USA

²Department of Pediatrics, Hasbro Children's Hospital, Warren Alpert Medical School of Brown University, Providence, RI, USA

³Department of Anesthesia, Children's Hospital Boston, Harvard Medical School, Boston, MA, USA

⁴Department of Orthopedics, Children's Hospital Boston, Harvard Medical School, Boston, MA, USA

⁵Center for Advanced Orthopaedic Studies, Department of Orthopaedic Surgery, Beth Israel Deaconess Medical Center, Harvard Medical School, Boston, MA, USA

⁶Clinical and Translational Study Unit, Children's Hospital Boston, Boston, MA, USA

⁷Division of Gastroenterology and Nutrition, Children's Hospital Boston, Harvard Medical School, Boston, MA, USA

⁸Department of Biostatistics and Computational Biology, Dana-Farber Cancer Institute, Boston, MA, USA

⁹Department of Biostatistics and Computational Biology, Dana-Farber Cancer Institute, Harvard School of Public Health, Boston, MA, USA

¹⁰Department of Radiology, Children's Hospital Boston, Harvard Medical School, Boston, MA, USA

¹¹Division of Genetics, Children's Hospital Boston, Harvard Medical School, Boston, MA, USA

¹²Division of Pediatric Oncology, Dana-Farber Cancer Institute and Children's Hospital Boston, Boston, MA, USA

ABSTRACT

Hutchinson-Gilford progeria syndrome (HGPS) is a rare segmental premature aging disorder that affects bone and body composition, among other tissues. We sought to determine whether bone density and structural geometry are altered in children with HGPS and whether relationships exist among these parameters and measures of skeletal anthropometry, body composition, and nutrition. We prospectively enrolled 26 children with HGPS (ages 3.1 to 16.2 years). Outcomes included anthropometric data; bone age; areal bone mineral density (aBMD) and body composition by dual-energy X-ray absorptiometry (DXA); volumetric bone mineral density (vBMD), strength-strain index (SSI), and bone structural rigidity calculated from radial transaxial peripheral quantitative computed tomographic (pQCT) images; serum bone biomarkers and hormonal measures; and nutrition assessments. Children with HGPS had low axial aBMD Z-scores by DXA, which improved after adjustment for height age, whereas differences in radial vBMD by pQCT were less striking. However, pQCT revealed distinct abnormalities in both novel measures of bone structural geometry and skeletal strength at the radius compared with healthy controls. Dietary intake was adequate, confirming that HGPS does not represent a model of malnutrition-induced bone loss. Taken together, these findings suggest that the phenotype of HGPS represents a unique skeletal dysplasia. © 2011 American Society for Bone and Mineral Research.

KEY WORDS: BONE QCT; CLINICAL/PEDIATRICS; BONE DENSITOMETRY; OSTEOPOROSIS; BONE MINERALIZATION

Introduction

Hutchinson-Gilford progeria syndrome (HGPS) is a rare sporadic autosomal dominant disorder that represents a segmental model of premature aging affecting multiple tissues, including bone and body composition. The disease locus for classic HGPS is on a limited region of chromosome 1q, a single recurrent de novo heterozygous point mutation most frequently

identified as p.G608G within exon 11 of the *LMNA* gene.^(1–3) The *LMNA* gene normally encodes for the protein lamin A, and in HGPS, production of both normal lamin A and the mutant protein progerin results.⁽⁴⁾ The cellular defects in HGPS stem from accumulation of progerin, which leads to nuclear membrane distortion and a decreased cellular life span. Bony defects may be secondary to accumulation of progerin within skeletal tissue.⁽⁵⁾

Received in original form December 3, 2010; revised form January 26, 2011; accepted March 17, 2011. Published online March 28, 2011.

Address correspondence to: Catherine M Gordon, MD, MSc, Divisions of Adolescent Medicine and Endocrinology, Children's Hospital Boston, 300 Longwood Avenue, Boston, MA 02115, USA. E-mail: catherine.gordon@childrens.harvard.edu

Journal of Bone and Mineral Research, Vol. 26, No. 7, July 2011, pp 1670–1679

DOI: 10.1002/jbmr.392

© 2011 American Society for Bone and Mineral Research

Patients with the classic gene mutation for HGPS have a normal appearance at birth and progressively develop strikingly similar signs and symptoms by the age of 1 year.^(6,7) The phenotype is characterized by alopecia, significant loss of subcutaneous fat, lack of weight gain, and extreme short stature, among other features. Skeletal manifestations include osteolysis, contractures, coxa valga, and shortened clavicles.^(6,8) An irregular pattern of mineralization has been described, especially at the distal metaphyses of long bones.⁽⁶⁾ In 41 children with HGPS followed longitudinally, no increased fracture rate was noted, and a unique growth pattern was identified, including slow weight gain averaging 0.52 kg/year by age 2 years and remaining linear thereafter. Maximum lifetime weight and height are usually well under 20 kg and 100 cm, respectively.

To our knowledge, no previous studies of children with HGPS have quantitatively evaluated both their bone mineral density (BMD) and structural geometry. We determined whether reduced mineralization was present by measuring whole-body and spinal areal bone mineral density (aBMD) using dual-energy X-ray absorptiometry (DXA), including adjustments for height age, and bone age. We also used peripheral quantitative computed tomographic (pQCT) images of the radius to evaluate both the material and geometric properties of the bone by measuring volumetric bone mineral density (vBMD), an estimate of bone bending strength [strength-strain index (SSI)], and bone structural rigidity.^(9,10) Rigidity is an engineering parameter that integrates both the material and geometric properties of the bone; the axial, bending, and torsional rigidity determine the capacity of the bone to resist axial loads, bending, and twisting moments, respectively. We also investigated the character and mechanism of bone disease by evaluating dietary intake and energy utilization. A prior natural history study in HGPS revealed adequate caloric intake.⁽⁸⁾ Therefore, we sought to confirm and expand this finding by carrying out a detailed nutritional evaluation and obtaining body composition measures to determine whether HGPS represented a model of malnutrition-induced bone loss. Lastly, we measured concentrations of bone biomarkers to determine whether this disease represents a state of high bone turnover, as is associated with aging.

Methods

Participant selection

Twenty-six children aged 3 to 16 years (15 girls and 11 boys) were enrolled with classic p.G608G HGPS (1824 C > T on *LMNA*).⁽³⁾ Entry criteria included clinical evidence of progeria and genetic diagnosis of HGPS by mutational analysis. To provide normative reference data for the pQCT measures, 57 normal controls were enrolled who were age- and gender-matched to the children with HGPS. The Children's Hospital Boston Committee on Clinical Investigation approved the study protocol. Written informed consent was obtained from the parents of all minors and study assent from children age 7 years and older. Participants were flown to a single study site from 16 different countries and spoke a total of nine different languages. Consent was provided in

written and oral forms in the language of origin, and translators were provided during all testing periods for non-English-speaking participants.

Study design

For HGPS participants, data were obtained prior to drug therapy during the baseline visit of a single-center, open-label treatment trial conducted in the Clinical and Translational Study Unit of Children's Hospital Boston. The study is registered with Clinicaltrials.gov at www.clinicaltrials.gov/ct2/show/NCT00916747?term=progeria&rank=1. Clinical histories were obtained using retrospective chart information provided by The Progeria Research Foundation Medical and Research Database (www.progeriaresearch.org/medical_database.html), and a complete history and physical were performed on site.

Study assessments

Areal bone mineral density (aBMD) of the total body (including head) and lumbar spine (L₁–L₄) by DXA (QDR Discovery A, Hologic, Inc., Bedford, MA, USA) was measured at one time point. Measurements were compared with age- and gender-matched controls using pediatric reference software.⁽¹¹⁾ With this instrument, the average in vivo precision for aBMD (expressed as percent coefficient of variation) for the DXA technologists was 0.62% at the spine and 0.72% at the total hip. A bone-age radiograph was obtained and interpreted using the Gruelich and Pyle atlas by one radiologist (RC).⁽¹²⁾ Height-age calculations were performed by one pediatric endocrinologist (CMG) using the median height obtained from Centers for Disease Control and Prevention growth charts (age at which subject's height corresponded to the 50th percentile). For height-age calculations, we used segmental whole-body lengths because joint contractures inherent to HGPS can result in an underestimation of true height. To generate adjusted BMD Z-scores, the height age or bone age was entered into the scanner, replacing the chronologic age.

pQCT bone measures of the left radius were obtained at the 4%, 20%, 50%, and 66% sites using a Stratec XCT 3000 device with a 12-detector unit, voxel size of 0.4 mm, slice thickness of 2.3 mm, and scan speed of 25 mm/s (Stratec AG, Birkenfeld, Germany). A scout view was obtained to place the reference line at the 4% site of the radius, adjacent to the growth plate, and measurements were obtained at the four specified percentages of radial length proximal to the reference line. Scans were analyzed using Stratec software, Version 5.50. The assessment sites were chosen given that a pattern of irregular reduced mineralization was noted by Gordon and colleagues in a previous study of HGPS.⁽⁶⁾ An indicator of bending strength, polar SSI, also was estimated at the 20%, 50%, and 66% sites.

In addition to measures of vBMD (grams of mineralized bone tissue per apparent cubic volume of bone tissue), pQCT was performed at serial cross sections through the radius, reflecting the structural properties of the metaphysis (comprised principally of cancellous bone—4% of bone length from the distal epiphysis), metadiaphysis (20% of bone length from the distal epiphysis), and diaphysis (comprised principally of cortical bone—50% and 66% of bone length from the distal epiphysis).

Although bone is composed of mineral, organic matrix, and water, computed tomography primarily reflects the attenuation signature of the mineral phase. Therefore, the density measured with quantitative computed tomography approximates the density of the mineral phase, or the ash density (ρ_{ash} , in mg/cm^3). A solid hydroxyapatite phantom containing three known mineral densities (480.6, 557.0, and 699.9 mg/cm^3) was imaged first using the same imaging protocol as for the radii. Linear regression between the attenuation coefficient and the corresponding ash densities for the phantom was performed. These regression equations were used to convert the X-ray attenuation of the pixels forming the bone cross section in the CT image to an equivalent ash density for each pixel corresponding to bone tissue. The modulus of elasticity (in MPa; i.e., the intrinsic stiffness of the bone tissue for each pixel in the image corresponding to bone) was calculated from the ash density using empirically derived relationships.^(13,14) The axial, bending, and torsional rigidities corresponding to each cross-sectional CT image through the bone were calculated by summing the modulus-weighted area of each pixel comprising the bone by its position relative to the modulus-weighted centroid of the bone in the cross section, according to standard structural engineering principles (composite beam theory) that have been validated extensively ex vivo and in vivo in both animal and human models.^(9,10,15)

Fasting venous blood samples were collected for measurement of the bone-formation marker, osteocalcin, and hormonal concentrations [25-hydroxyvitamin D [25(OH)D], parathyroid hormone (PTH), insulin-like growth factor I (IGF-I), and insulin-like growth factor-binding protein 3 (IGFBP3)]. A clean-catch urine (second morning void) was collected for measurements of the bone-resorption marker N-telopeptides (NTX).

Food records

Each participant's parent(s) completed a 7-day food record and submitted relevant food package labels to assist with tracking nutritional intake. A research dietitian (NQ) met with each family during the hospital visit to review the record for accuracy. For non-English-speaking participants, an interpreter assisted in translating the food record into English. The nutrient analysis program Nutrition Data System for Research (University of Minnesota, Minneapolis, MN, USA) was used to calculate mean daily nutrient intakes for each participant.

Statistical analysis

Data are presented as mean \pm SD unless otherwise indicated. Data are summarized using descriptive statistics (mean, standard deviation, maximum, minimum, and frequencies). Statistical comparisons between genders, age groups, or cases/controls were conducted using *t* tests for normally distributed data or Wilcoxon rank-sum tests for data where the SDs between groups were not approximately equal. Spearman correlation analyses and multivariable regression were used to identify significant predictors of skeletal outcomes. Statistical significance was defined as $p < .05$ with no corrections for multiple comparisons.

Results

Sample characteristics and anthropometric data

Twenty-six children with G608G classic HGPS were enrolled (ages 3.1 to 16.2 years). The average age of participants was 7.5 ± 3.2 years, with an average height age of 3.4 ± 1.6 years (on average, 4.1 years younger than chronologic age). Subjects had a low mean body mass index (BMI) of $11.5 \pm 1.2 \text{ kg}/\text{m}^2$ and mean weight of $10.46 \pm 2.7 \text{ kg}$. There was no significant difference for BMI or weight between the boys and girls.

Seventeen children with HGPS required BMD Z-score adjustments for height age. We designed the study such that a height-age adjustment was not made if either the subject's height age was within 1 year of the chronologic age ($n = 0$) or below age 3 years (ie, pediatric reference software for DXA was not available for age ≤ 2 years; $n = 9$). One child was missing data for bone age, resulting in a sample size of 25 for that measurement.

Comparisons of bone and height ages in the full sample and within gender subgroups are shown in Table 1. The average bone age was 7.7 ± 3.8 years, which was not statistically different from chronologic age ($p > .05$). However, there was significant variability such that 5 of 24 (21%) of the patients had a delayed bone age, 9 of 24 (38%) of the patients had an advanced bone age, and 10 of 24 (41%) of the patients were within the established SD for chronologic age. When compared with chronologic age, the boys had slightly more advanced bone age than the girls (ie, the mean bone age of the boys was almost 1 year greater than their chronologic age, whereas girls showed no difference).

In contrast to bone age, height age was at least 1 year below chronologic age in all 26 children. When summarized across age groups, older children (ages 10 to 17 years) had a greater deficit than younger children (ages 3 to 9 years) in the comparison of height age with chronologic age (-6.5 years versus -3.9 years, $p = .01$).

Three participants (12%) had a history of fractures, each of which occurred in the setting of trauma, with four total fractures reported for the sample (ie, fibula, radius, and two skull fractures). The reported healing rate was normal, which was confirmed on X-rays for all the fractures.

DXA-areal bone mineral density

In order to interpret bone density measured by DXA in the context of a disease where extremely small size and/or altered bone age may influence the analysis, we assessed aBMD in three ways: unadjusted, height-age adjusted, and bone-age adjusted (Table 2). In the majority of subjects, unadjusted aBMD was low at the spine and whole body, defined as a BMD Z-score of -2 SD or less, a significant threshold established by expert consensus for the pediatric age group.⁽¹⁶⁾ We found unadjusted aBMD Z-scores of less than -2 SD for 22 of 25 (88%) patients at the lumbar spine and 24 of 24 (100%) at the whole body. Comparisons by gender showed that girls had significantly lower lumbar spine Z-scores at baseline (Wilcoxon rank-sum $p = .04$), although Z-scores were low for both genders. There were no differences between boys and girls for the whole body ($p > .05$).

Table 1. Height Age and Bone Age by Gender

	<i>n</i>	Mean	SD	Min	Max
Chronological age (years)					
Total	26	7.5	3.2	3.1	16.2
Female	15	7.1	3.3	3.1	16.2
Male	11	8.1	2.9	3.2	11.6
Height age (years)					
Total	26	3.4	1.6	1.0	7.0
Female	15	3.0	1.4	1.0	6.5
Male	11	4.0	1.7	2.0	7.0
Height-age comparison (baseline – chronologic) (years)					
Total	26	–4.3	2.0	–9.6	–1.3
Female	15	–4.0	2.2	–9.6	–1.3
Male	11	–4.6	1.8	–6.9	–1.3
Bone age (years)					
Total	24	7.7	3.8	2.0	17.0
Female	15	7.2	3.8	2.5	17.0
Male	9	8.7	3.9	2.0	12.5
Bone-age comparison (baseline – chronologic) (years)					
Total	24	0.4	1.6	–3.8	4.1
Female	15	0.1	1.1	–2.3	2.0
Male	9	0.8	2.2	–3.8	4.1

aBMD Z-scores of the spine and total body then were adjusted for height age and bone age (Table 2). Bone-age adjustment did not significantly affect aBMD Z-scores owing to the similarity between bone age and chronologic age (Table 1). However,

several bone-related measures were significantly different between boys and girls. Girls had lower bone-age-adjusted Z-scores of the spine ($p = .01$; Table 2), corresponding to the fact that the girls had significantly younger bone ages ($p = .048$;

Table 2. Adjusted and Unadjusted aBMD Z-Scores by DXA (in SD)

	<i>n</i>	Mean	SD	Minimum	Maximum
Spine unadjusted					
Female	14	–3.38	0.95	–5.00	–1.90
Male	11	–2.55	0.93	–4.10	–0.80
Overall	25	–3.02	1.01	–5.00	–0.80
Spine height-age-adjusted					
Female	7	–1.54	1.73	–3.40	1.40
Male	5	–2.12	1.07	–3.40	–1.10
Overall	12	–1.78	1.46	–3.40	1.40
Spine bone-age-adjusted					
Female	7	–4.23	0.46	–4.60	–3.30
Male	7	–2.89	0.98	–4.00	–1.10
Overall	14	–3.56	1.01	–4.60	–1.10
Total body unadjusted					
Female	13	–4.17	0.85	–5.60	–3.00
Male	11	–4.50	0.92	–5.90	–3.30
Overall	24	–4.32	0.88	–5.90	–3.00
Total body height-age-adjusted					
Female	6	–2.32	0.96	–3.20	–0.60
Male	5	–2.96	0.91	–3.80	–1.80
Overall	11	–2.61	0.95	–3.80	–0.60
Total body bone-age-adjusted					
Female	7	–4.91	0.46	–5.80	–4.50
Male	7	–5.33	0.90	–6.30	–3.90
Overall	14	–5.12	0.72	–6.30	–3.90

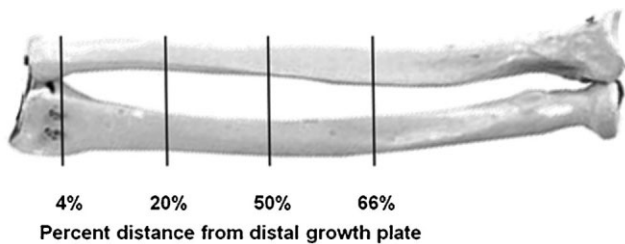


Fig. 1. Skeletal sites assessed via peripheral quantitative computed tomography. Cross-sectional measures were obtained 4%, 20%, 50%, and 66% distance from distal growth plate.

Table 2), as well as smaller differences between bone age and chronologic age ($p = .006$; Table 2).

Most impressive was the attenuation of the apparent deficit in bone mass initially suggested by the unadjusted aBMD. When the data were modified to reflect height age, Z-scores rose at both the spine and total body by +1.24 and +1.71 SD, respectively.

DXA-body composition

The reported mean percentage body fat by DXA was $16.1\% \pm 4.8\%$. There were no differences noted between boys and girls with respect to total fat mass, but there was a trend toward boys having higher lean body mass than girls (9834.60 ± 2950.24 g versus 7393.93 ± 1894.71 g, $p = .08$).

Total fat mass was positively correlated with unadjusted lumbar spine BMD ($r = 0.49$, $p = .01$) and the bone-age-adjusted spinal Z-score ($r = 0.56$, $p = .04$). Lean body mass was positively correlated with unadjusted total-body ($r = 0.76$, $p < .001$) and spinal BMD ($r = 0.65$, $p = .0003$). Including all children in the sample, there were strong, significant positive correlations between lean tissue mass and both unadjusted total-body BMD ($r = 0.762$, $p < .0001$) and unadjusted spinal BMD ($r = 0.654$, $p = .003$).

pQCT measurements of bone morphology, vBMD, structural rigidity, and strength-strain index (SSI)

We evaluated bone morphology, density, and structure in children with HGPS using transaxial pQCT images acquired at four sites along the radius (Fig. 1). Morphologically, we found

dramatic abnormalities in some of the children with HGPS, where the cross-sectional images revealed either a starred or hooked morphology, as well as abnormally narrow medullary cavities (Fig. 2). Five of 26 (19%) of the HGPS cohort and none of the healthy control patients possessed star- or hooklike morphologic abnormalities.

Since there are no age-defined normal reference data for vBMD, SSI, and structural rigidity determined from transaxial pQCT images of the radius in the literature, we enrolled 57 age- and gender-matched control children to be compared with the HGPS children.

The axial (EA), bending (EI), and torsional (GJ) rigidities were calculated from the transaxial pQCT images of the radius at the metaphysis (comprised principally of cancellous bone) and the metadiaphysis and diaphysis (comprised principally of cortical bone; Fig. 3). Structural rigidity variables were dramatically abnormal at all sites compared with the age- and gender-matched normal control group. Axial rigidity of the radii of the HGPS patients was on average 40% lower than those of control subjects ($p < .0001$ at all four radial sites). Bending and torsional rigidities of the radii of the HGPS patients were on average 66% lower than controls ($p < .0001$ at all four radial sites).

In children with HGPS, total vBMD measured by pQCT was comparable with that of the normal controls throughout the radius (Fig. 3D). SSI also was calculated at the 20%, 50%, and 66% sites and was significantly lower in HGPS versus healthy controls at all three sites ($p < .0001$; Table 3).

Among the children with HGPS at the 20% site, the lean body mass measured by DXA was correlated with total vBMD ($r = 0.67$, $p = .0005$).

Biochemical measures

To understand the mechanisms mediating the skeletal abnormalities in HGPS, we measured bone turnover and other markers of bone metabolism compared with age-matched reference data (Table 4). Mean serum osteocalcin, a bone-formation marker, was in the high-normal range for both the boys and girls.⁽¹⁷⁾ Mean urinary NTX concentrations, representing surrogate markers of bone resorption, were highly variable. Nineteen of the 26 children had normal NTX concentrations (73.1%, 12 girls, 7 boys), 3 children had abnormally high levels (11.5%, 1 girl, 2 boys), and

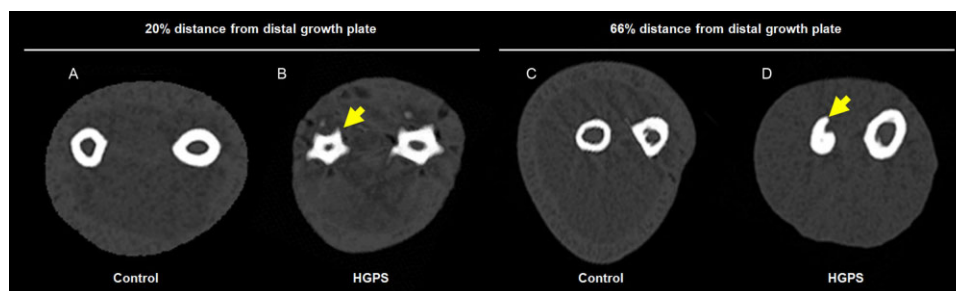


Fig. 2. Differences in bone structure and geometry in patients with Hutchinson-Gilford progeria syndrome (HGPS) versus healthy controls. This figure outlines some of the unusual cross-sectional geometries observed in the HGPS patients. The left panel highlights a star-shaped cross section for the radius and ulna at 20% distance from the distal growth plate in comparison with the more elliptical cross sections of the bones from a control subject. The panel on the right denotes a tailed ulnar cross section at a distance of 66% from the distal growth plate, where the medullary cavity is filled with bone. This is in sharp contrast to the site-matched cross-section from a control subject.

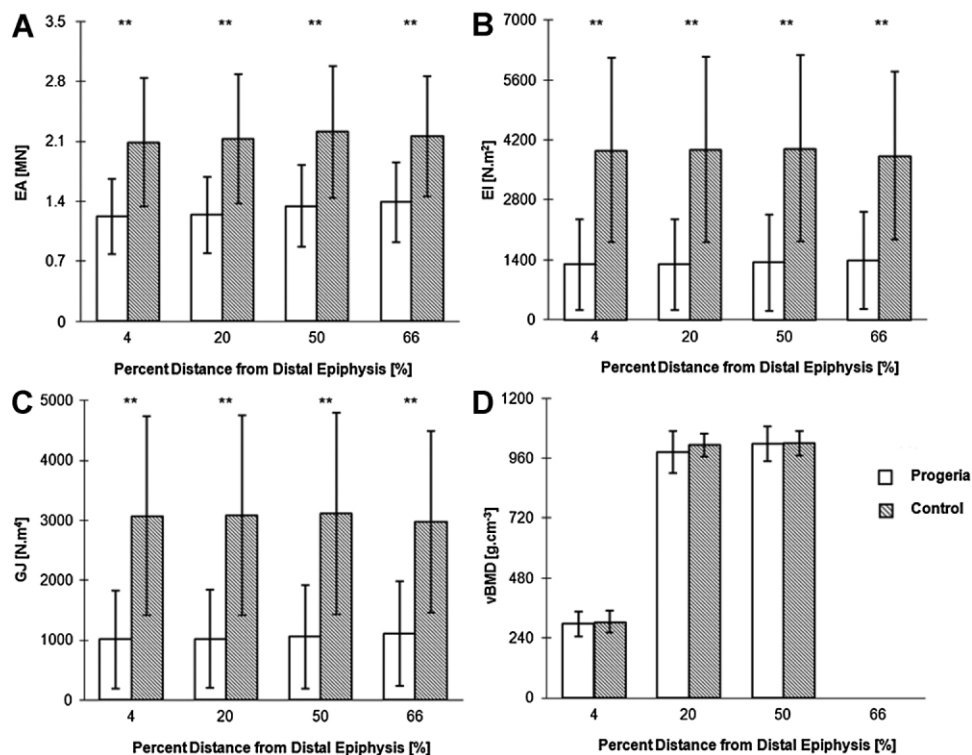


Fig. 3. Differences in skeletal rigidity in patients with HGPS versus healthy controls. Means and SD for (A) cross-sectional axial (EA), (B) bending (EI), and (C) torsional (GJ) rigidities and (D) total vBMD at indicated radial sites in patients with HGPS (white bars) and matched control patients (gray bars). **p* < .0001.

4 children had abnormally low levels (15.4%, 2 girls, 2 boys).⁽¹¹⁾ Mean IGF-1 and IGFBP3 were normal for age, even when data from the five children receiving recombinant growth-hormone therapy (whose values were expectedly higher than untreated subjects) were included (Table 4). A host of additional measures of bone metabolism were within normal limits and were comparable between boys and girls.

Nutrition

Table 5 summarizes daily nutrient intakes compared with age-matched recommended daily allowances (RDAs) for the HGPS participants.⁽¹⁸⁾ Although RDAs are designed for much larger children for each age comparison, all participants received at least 95% of the RDA for energy intake. The RDA is defined as the

average daily dietary nutrient intake level sufficient to meet the nutrient requirement of 97% to 98% of healthy individuals for a particular life stage and gender group. Energy intake was not significantly correlated with weight, height, body mass index, or lean body mass. Protein, calcium, and vitamin D intakes also met or exceeded the RDAs in the majority of participants (Table 5). Mean protein intake was 15% of daily energy intake (range 10% to 25%). All participants received at least 84% of the RDA for protein, and 75% of participants had protein intakes at least 40% higher than the RDA. Mean carbohydrate intake was 52% of daily energy intake. Thirty-one percent of participants (8 of 26) had a calcium intake at or above the RDA. Vitamin D deficiency [serum 25(OH)D ≤ 20 ng/mL] was present in 3 (12%) participants, and insufficiency [25(OH)D ≤ 30 ng/mL] was present in 8 (31%).

Table 4. Bone Turnover and Endocrine Measures

Test ^a	Females (<i>n</i> = 15)		Males (<i>n</i> = 10) ^b		Overall (<i>n</i> = 25) ^b		Age-appropriate normal range
	Mean	SD	Mean	SD	Mean	SD	
Osteocalcin (ng/L)	43.20	19.60	50.90	13.38	46.28	17.49	5–30
<i>N</i> -Telopeptides (nmol/mmol Cr)	312.80	166.14	333.91	259.21	321.73	206.03	F: 123.6–544.0 M: 136.6–426.8
IGF-1 (ng/mL)	158.31	81.45	220.13	190.56	183.04	135.81	(ref) ^c
IGFBP3 (mg/L)	2.97	1.06	3.04	0.98	3.00	1.01	(ref) ^c
Calcium (mg/dL)	10.00	0.30	9.95	0.36	9.98	0.32	8.0–10.5
Phosphorus (mg/dL)	5.07	0.55	4.83	0.57	4.97	0.56	1–13 y/o = 3–5.7 >13 y/o = 2.7–4.9
Alkaline phosphatase (U/L)	142.67	43.64	144.70	53.86	143.48	46.90	(ref) ^c
Total protein (g/dL)	7.53	3.47	7.15	0.57	7.38	2.68	5.5–8.2
25-hydroxyvitamin D (ng/mL)	34.20	13.16	34.40	13.23	34.28	12.91	30–80
Parathyroid hormone (pg/mL)	11.57	6.12	13.20	6.47	12.22	6.18	10–65

^aAll tests are serum measures except *N*-telopeptides, which are urinary measures.

^bFor *N*-telopeptides, *n* = 11 males and overall = 26.

^cNormal ranges vary widely with age and/or gender.

Discussion

HGPS is a disease of dramatic short stature and unique radiographic findings such as acroosteolysis, shortened clavicles, coxa valga, and decreased mineralization at the distal metaphyses of long bones in the face of normal fracture rates.⁽⁶⁾ To gain a more complete understanding of the nature of the skeletal abnormalities and their pathogenesis, we performed an extensive anatomic and functional skeletal evaluation of 26 children with HGPS. We arrived at a new understanding of bone pathology in HGPS that required the integration of assessments using DXA, pQCT, bone turnover markers, and analysis of nutritional intake. The findings demonstrate a unique skeletal dysplasia whose pathogenesis does not lie within a picture of defective bone turnover or malnutrition.

We first measured bone density by DXA. In agreement with previously published data,⁽⁸⁾ our unadjusted *Z*-scores were

extremely low in all children with HGPS, yet fracture rates were low in the face of normal daily physical activity. Adjustments for bone age did not significantly influence aBMD *Z*-scores because bone age was variable and overall was not significantly different from chronologic age. However, since DXA measures the X-ray attenuation of bone over a user-specified areal region of analysis and fails to account for variation in the out-of-plane dimension of bone, it provides only a 2D measurement of “bone density”; therefore, it can be confounded by differences in bone size. Children with HGPS exhibit a characteristic lack of weight gain and growth arrest by 2 years of age.⁽⁶⁾ Thus we hypothesized that comparing their DXA measures of aBMD with reference data matched for chronologic age would result in an overestimate of deficits in skeletal mineral mass. In our study, these children had a height age that lagged by an average of 4 years. Although correction for height age still resulted in low aBMD *Z*-scores, the mean scores rose from an extremely low range to that consistent

Table 5. Daily Caloric and Nutrient Intake Versus RDA (*n* = 26)

	Mean	SD	% of RDA, mean	% of RDA, SD	% RDA, minimum	% RDA, maximum
Energy (kcal) overall	1222.40	271.93	158.67	46.30	95.70	278.84
F (<i>n</i> = 15)	1138.20	255.34	152.57	38.84	95.70	239.96
M (<i>n</i> = 11)	1337.18	261.63	166.99	55.81	96.29	278.84
Total fat (g)	47.16	17.41	87.13	37.33	23.33	182.76
Total carbohydrate (g)	156.01	34.47	120.01	74.10	120.81	186.13
Total protein (g)	46.87	17.63	226.84	100.86	83.82	434.74
Vitamin K (μg)	32.28	13.77	67.84	40.84	18.38	230.50
Vitamin C (mg)	58.42	38.10	129.83	84.66	17.69	336.64
Vitamin D (IU)	216.95	147.54	108.48	73.77	22.00	321.00
Calcium (mg)	677.50	406.10	83.33	54.65	25.28	264.56
Phosphorus (mg)	810.95	317.53	126.76	55.96	35.27	216.02
Magnesium (mg)	150.86	54.99	108.52	53.41	43.25	270.63
Zinc (mg)	8.04	4.23	161.24	109.30	42.88	511.33
Copper (mg)	0.84	0.48	170.30	88.08	71.43	367.65

with the normal fracture rate seen in these children. These data underscore the importance of accurately assessing BMD status as a biomarker of disease in HGPS.

To investigate our hypothesis that HGPS represents a skeletal dysplasia affecting the structural geometry of the appendicular skeleton rather than a premature loss of bone mass, we used transaxial pQCT images at four regions along the radius to evaluate quantitatively both the material and geometric properties of the bone. We measured both vBMD and bone structural rigidity. The latter parameter integrates the material and geometric properties of bone that govern its capacity to resist applied loads. Since there are sparse pediatric normative data for pQCT-derived vBMD, SSI, or structural rigidity measures, we enrolled healthy control subjects for comparison. Given that vBMD represents a true 3D measure of apparent bone mineral mass density that is not subject to size differences, only age and gender were matched in this evaluation. In contrast to the low aBMD Z-scores reported at the axial skeleton using DXA, total vBMD evaluated at serial cross sections through the radius using pQCT was not significantly different from that of healthy controls. However, we discovered dramatic geometric abnormalities in some subjects with HGPS such as hooked and starred phenotypes that have not been described previously. These striking structural changes may account for the abnormally distributed bone mineralization observed in the appendicular skeleton of children with HGPS on plane radiographs.⁽⁶⁾ The clinical significance of these novel findings, including their impact on long-term skeletal strength and fracture risk, merits further study. Use of more sophisticated skeletal assessment tools such as high-resolution pQCT is also needed to understand the prevalence and etiology of the abnormal morphologies noted and their functional implications.

The capacity of a bone to support load depends on its structural properties, which are determined by the material properties of bone tissue and how that tissue is distributed in space. Rigidity is the structural property that governs the ability of a bone to resist axial loads, bending, and torsional moments; it is the integral product of the bone tissue modulus (which is a function of the BMD) and bone cross-sectional geometry and was highly abnormal in HGPS compared with healthy controls. pQCT was performed at serial cross sections through the radius to provide assessments of trabecular and cortical bone. We employed a CT-based method to calculate the cross-sectional axial ($EA = \text{integral of modulus of elasticity and cross-sectional area}$) bending ($EI = \text{integral of modulus of elasticity and moment of inertia}$) and torsional ($GJ = \text{integral of shear modulus and polar moment of inertia}$) rigidities at the radius,^(9,10) as well as SSI, which is an additional indicator of bone-building strength.⁽¹⁹⁾ SSI reflects the elastic modulus properties of bone and results from a weighted bone strength analysis. The axial rigidity of HGPS children was 40% less at the metaphysis and diaphysis of the radius, and the bending and torsional rigidities were 66% less than in normal controls. SSI also was significantly lower in the patients with HGPS versus healthy control subjects at all regions of the radius. Therefore, HGPS appears to affect primarily the structural geometry, suggestive of a skeletal dysplasia.

Additional support for a skeletal dysplasia in HGPS includes the atypical pattern of reduced mineralization noted in the long

bones of these children, including progressive focal changes as opposed to global skeletal losses that may occur with aging.⁽⁶⁾ Another unique finding was that while diaphyseal cortical regions appear to be normal in these children, there was decreased mineralization noted at the metaphyses. The trend toward an advanced bone age observed in these children is also a pattern that has been noted in other skeletal dysplasias.⁽²⁰⁾ Finally, other data supporting a skeletal dysplasia include characteristic skeletal findings such as clavicular resorption, coxa valga, and acroosteolysis, among others, as have been reported previously.^(6,8) Inevitably, the lack of weight gain and growth delay in these children induces body composition changes that result in a much lighter skeletal load. Therefore, some of the abnormalities in bone density, structure, and strength observed may represent an adaptive response.

In non-HGPS populations, malnutrition often leads to decreased bone formation such as that seen in patients with the disease anorexia nervosa.⁽²¹⁾ Since patients with HGPS have extremely low subcutaneous fat, it has been assumed that these patients consume diets inadequate in macro- or micronutrients, predisposing them to bone loss and that this disease represents a pediatric model of malnutrition-induced bone loss. Our data suggest the contrary because the majority of children with HGPS had intakes of energy, protein, calcium, and vitamin D that were adequate to support normal bone mineralization, weight gain, and linear growth. Neither energy nor protein intake was associated with measures of body composition, suggesting that increasing energy or protein intake had no effect on growth enhancement in these children. Finally, bone biomarker data, suggesting normal bone formation and turnover, provided additional evidence that the bone loss seen is not secondary to malnutrition.

In considering whether HGPS, a presumed model of early aging, represents senile osteoporosis, an examination of bone turnover was informative. A hallmark finding in senile osteoporosis is increased bone resorption,⁽²²⁾ although not always involving high bone remodeling.⁽²³⁾ The primary pathophysiology in aging includes too few osteoblasts to replace the bone removed by osteoclasts during remodeling. Markedly increased bone resorption leads to the initial fall in bone density seen in the elderly. With increasing age, there is also a significant reduction in bone formation. The pattern noted in this sample of HGPS patients was different. In these young patients, bone formation, as reflected by osteocalcin levels, was in the high-normal range. Bone-resorption markers also were within a normal pediatric range for the majority of participants. Thus the usual biomarkers of senile osteoporosis, a multifactorial disease, may not apply in HGPS, where downstream effects of a single protein variant, progerin, is the primary cause of disease.

Progerin's expression in a variety of cell types leads to early cell death *in vitro*.⁽²⁴⁾ Human HGPS autopsies reveal progerin expression in all organs and abnormal extracellular matrix distribution in the vasculature.⁽²⁵⁾ We speculate that progerin accumulation in human osteocytes creates dysregulation of cell signaling and a toxic environment that culminates in abnormal bone growth and cell death. This underlying cellular activity ultimately may manifest as the measurable skeletal outcomes that encompass the HGPS skeletal phenotype, including subtle

abnormalities in bone density and more striking alterations in skeletal geometry and structure. Mouse model studies support this hypothesis as well. Progerin is expressed in the osteocytes of mouse models of HGPS^(26,27) and can lead to bony abnormalities that are ameliorated with farnesyltransferase inhibitors, drugs that affect progerin's retention in the inner nuclear membrane.⁽²⁶⁾ Similarly, statins and aminobisphosphonates inhibit both farnesylation and geranylgeranylation of progerin and prelamin A and markedly improve the lifespan and bony abnormalities in progeroid mice engineered to accumulate prelamin A (a protein with similarities to progerin).⁽²⁸⁾ Clinical trials are under way to understand the effects of these promising regimens on bone and other tissues.

Study limitations deserve acknowledgment and reconsideration. Our sample was limited owing to the rarity of this disorder (frequency 1 in 4 million). Nonetheless, it represents the largest sample size to date, with attempts made to include all children known to have the disorder who were well enough to travel and participate in the study. Another limitation was possible misclassification of specific nutrient intakes owing to our reliance on a U.S. food composition database; such misclassification may have biased our results toward the null. For participants residing in foreign countries, different fortification standards may have led to over- or underestimation of micronutrient intakes in particular. To minimize misclassification, we entered into our database food composition data from food labels supplied by participants. Measurements of aBMD provide a 2D estimate of bone density and do not yield information regarding skeletal strength or microarchitecture. Therefore, we simultaneously obtained pQCT measures of vBMD at the radius and calculated novel measures of skeletal structure that integrate both the tissue material properties and cross-sectional geometric aspects of bone. SSI was significantly low in HGPS, but this measure assumes homogeneous tissue properties, and we discovered heterogeneity in the bone structure of children with HGPS. Measures of EI were especially important because it is derived using the composite-beam theory and models bone mass distribution in space without assuming homogeneous tissue properties. Therefore, the combined information we obtained provided a more comprehensive assessment of bone health in these children. Future studies should examine these properties in the lower extremities and spine, in addition to the radius, and techniques such as high-resolution pQCT would enable a better evaluation of bone microarchitecture. We acknowledge the presence of potential motion artifact in the pQCT measures that was difficult to avoid in some of the youngest patients, as well as those with severe contractures. However, including younger patients allowed us to assess HGPS in the broadest age and disease-stage cohort possible, and SDs remained within acceptable limits for the cohort. Lastly, we acknowledge the limitations of a single spot sample for the NTX measurements and both potential assay imprecision and confounding owing to varying growth rates among the participants.

In summary, the growth and development of the skeleton are affected dramatically in children with HGPS, resulting in a unique skeletal dysplasia with bone morphologic abnormalities and short stature. Bone density measures by DXA improved

dramatically when bone size was taken into account and were in the normal range by pQCT. However, there were significant bone structural alterations noted by pQCT. We have defined four new measures of abnormality in HGPS that characterize this dysplasia, namely, EA, EI, GJ, and SSI. These all should be considered as indicators of bone status in HGPS that can be used to evaluate skeletal disease progression and improvements with prospective treatments in the future. The structural skeletal deficits seen are not consistent with senile osteoporosis or malnutrition-related bone loss because serum indices of bone remodeling were in the normal pediatric range, and there was no evidence of dysfunctional calcium homeostasis. The clinical implications of these abnormalities will be important to understand, especially as promising new therapies lead to an extended life span for these children.

Disclosures

LBG is the parent of a child with HGPS who participated in this study. All the other authors state that they have no conflicts of interest.

Acknowledgments

The study was funded by the Progeria Research Foundation (PRFCLIN2007-01), by NIH grants to the Children's Hospital Boston GCRC (MO1-RR02172), and by the Harvard Catalyst Clinical and Translational Study Unit (CTSU; UL1 RR025758-01). Additional support was provided by the Stop&Shop Family Pediatric Brain Tumor Program.

We are grateful to the children with progeria and their families, as well as the healthy control children, for their participation in this study. We also thank Yailka Cardenas, Kelly Littlefield, and Kiera McKendrick for excellent technical assistance and Christine Ploski, PT, MS, pCS, and Susan Riley, PT, MS, DPT, PCS, for providing segmental height measurements. Lastly, we gratefully acknowledge the outstanding care provided by the nursing staff of CTSU.

References

1. Cao H, Hegele RA. *LMNA* is mutated in Hutchinson-Gilford progeria (MIM 176670) but not in Wiedemann-Rautenstrauch progeroid syndrome (MIM 264090). *J Hum Genet.* 2003;48:271–274.
2. De Sandre-Giovannoli. Lamin A truncation in Hutchinson-Gilford progeria. *Science.* 2003;300:2055.
3. Eriksson M, Brown WT, Gordon LB, et al. Recurrent de novo point mutations in lamin A cause Hutchinson-Gilford progeria syndrome. *Nature.* 2003;423:293–2938.
4. Goldman RD, Shumaker DK, Erdos MR, et al. Accumulation of mutant lamin A causes progressive changes in nuclear architecture in Hutchinson-Gilford progeria syndrome. *Proc Natl Acad Sci USA.* 2004;101:8963–8968.
5. Capell BC, Erdos MR, Madigan JP, et al. Inhibiting farnesylation of progerin prevents the characteristic nuclear blebbing of Hutchinson-Gilford progeria syndrome. *Proc Natl Acad Sci USA.* 2005;102:12879–12884.

6. Gordon LB, McCarten KM, Giobbie-Hurder A, et al. Disease progression in Hutchinson-Gilford progeria syndrome: impact on growth and development. *Pediatrics*. 2007;120:824–833.
7. DeBusk FL. The Hutchinson-Gilford progeria syndrome. Report of 4 cases and review of the literature. *J Pediatr*. 1972;80:697–724.
8. Merideth MA, Gordon LB, Clauss S, et al. Phenotype and course of Hutchinson-Gilford progeria syndrome. *N Engl J Med*. 358:592–604.
9. Snyder BD, Cordio MA, Nazarian A, et al. Noninvasive prediction of fracture risk in patients with metastatic cancer to the spine. *Clin Cancer Res*. 2009;15:7676–7683.
10. Snyder BD, Hauser-Kara DA, Hipp JA, Zurakowski D, Hecht AC, Gebhardt MC. Predicting fracture through benign skeletal lesions with quantitative computed tomography. *J Bone Joint Surg Am*. 2006;88:55–70.
11. Kelly TL, Specker BL, Binkley T, et al. Pediatric BMD reference database for US white children. *Bone*. 2005;36 (Suppl 1): S30.
12. Greulich WW, Pyle SI. *Radiographic Atlas of Skeletal Development of the Hand and Wrist*. Stanford, CA: Stanford University Press, 1950.
13. Snyder S, Schneider E. Estimation of mechanical properties of cortical bone by computed tomography. *J Orthop Res*. 1991;9:422–31.
14. Rice JC, Cowin SC, Bowman JA. On the dependence of the elasticity and strength of cancellous bone on apparent density. *J Biomech*. 1988;21:155–168.
15. Whealan KM, Kwak SD, Tedrow JR, Inoue K, Snyder BD. Noninvasive imaging predicts failure load of the spine with simulated osteolytic defects. *J Bone Joint Surg Am*. 2000;82:1240–1251.
16. Gordon CM, Bachrach LK, Carpenter TO, et al. Special report on the 2007 Pediatric Position Development Conference of the International Society for Clinical Densitometry. *J Clin Densitom*. 2008;11:43–58.
17. Vietri MT, Sessa M, Pilla P, et al. Serum osteocalcin and parathyroid hormone in healthy children assessed with two new automated assays. *J Pediatr Endocrinol Metab*. 2006;19:1413–1419.
18. National Academy of Sciences. *Recommended Daily Allowances* 10th edition. Washington DC: National Academy Press, 1989.
19. Dowthwaite JN, Hickman RM, Kanaley JA, Ploutz-Snyder RJ, Spadaro JA, Scerpella TA. Distal radius strength: a comparison of DXA-derived vs pQCT-measured parameters in adolescent females. *J Clin Densitom*. 2009;12:42–53.
20. Kim OH, Nishimura G, Song HR, et al. A variant of Desbuquois dysplasia characterized by advanced carpal bone age, short metacarpals, and elongated phalanges: report of seven cases. *Am J Med Genet A*. 2010;152A:875–885.
21. DiVasta AD, Feldman HA, Quach AE, Balestrino M, Gordon CM. The effect of bed rest on bone turnover in young women hospitalized for anorexia nervosa: A pilot study. *J Clin Endocrinol Metab*. 2009;94:1650–1655.
22. Duque G, Troen BR. Understanding the mechanisms of senile osteoporosis: new facts for a major geriatric syndrome. *J Am Geriatr Soc*. 2008;56:935–941.
23. Manolagas SC. From estrogen-centric to aging and oxidative stress: a revised perspective of the pathogenesis of osteoporosis. *Endocr Rev*. 2010;31:266–300.
24. Bridger JM, Kill IR. Aging of Hutchinson-Gilford progeria syndrome fibroblasts is characterised by hyperproliferation and increased apoptosis. *Exp Gerontol*. 2004;39:717–724.
25. Olive M, Harten I, Mitchell R, et al. Cardiovascular pathology in Hutchinson-Gilford progeria: correlation with the vascular pathology of aging. *Arterioscler Thromb Vasc Biol*. 2010;30:2301–2309.
26. Fong LG, Frost D, Meta M, et al. A protein farnesyltransferase inhibitor ameliorates disease in a mouse model of progeria. *Science*. 2006;311:1621–1623.
27. Varga R, Eriksson M, Erdos MR, et al. Progressive vascular smooth muscle cell defects in a mouse model of Hutchinson-Gilford progeria syndrome. *Proc Natl Acad Sci U S A*. 2006;103:3250–3255.
28. Varela I, Pereira S, Ugalde AP, et al. Combined treatment with statins and aminobisphosphonates extends longevity in a mouse model of human premature aging. *Nat Med*. 2008;14:767–772.